

High visibility on-chip quantum interference of single surface plasmons

Yong-Jing Cai, Ming Li, Xi-Feng Ren*, Chang-Ling Zou, Xiao Xiong,
Hua-Lin Lei, Bi-Heng Liu†, Guo-Ping Guo‡, and Guang-Can Guo^{1,2}

¹Key Lab of Quantum Information, University of Science and Technology of China, CAS, Hefei, Anhui, 230026, China.

²Synergetic Innovation Center of Quantum Information & Quantum Physics,
University of Science and Technology of China, Hefei, Anhui 230026, China

Quantum photonic integrated circuits (QPICs) based on dielectric waveguides have been widely used in linear optical quantum computation. Recently, surface plasmons have been introduced to this application because they can confine and manipulate light beyond the diffraction limit. In this study, the on-chip quantum interference of two single surface plasmons was achieved using dielectric-loaded surface-plasmon-polariton waveguides. The high visibility (greater than 90%) proves the bosonic nature of single plasmons and emphasizes the feasibility of achieving basic quantum logic gates for linear optical quantum computation. The effect of intrinsic losses in plasmonic waveguides with regard to quantum information processing is also discussed. Although the influence of this effect was negligible in the current experiment, our studies reveal that such losses can dramatically reduce quantum interference visibility in certain cases; thus, quantum coherence must be carefully considered when designing QPIC devices.

Photonic integrated circuits (PICs), in which multiple photonic functional components comprise a single chip, have attracted considerable attention owing to their small footprints, scalability, reduced power consumption, and enhanced processing stability. In addition to their wide application in classical information processing, integrated photonic quantum logic gates and Shor's quantum factoring algorithm have been demonstrated on these chips [1, 2]; thus, they show great feasibility and high operation fidelity. More recently, much effort has been dedicated to surface plasmon polaritons (SPPs), which are electron density waves excited at the interface between a metal and a dielectric material [3] to further condense PICs beyond the diffraction limit. Not only can SPPs confine light at the nanoscale [4], they are also useful for integrated polarization-controlling devices [5, 6]. Studies using periodic metallic hole arrays provided the first experimental evidence that quantum entanglement can be preserved in the photon-SPP-photon conversion process [7–9]. Furthermore, the non-classical statistics of SPPs have been demonstrated using basic quantum Hong-Ou-Mandel (HOM) interference [10], in both long-range plasmonic waveguides (weakly confining waveguide) [11] and sub-wavelength metal plasmonic waveguides [12]. These studies indicate that assembling quantum PICs (QPICs) using plasmonic components is possible.

However, two obstacles remain that hinder the development of SPP-based QPICs. The first is that the experimental raw visibility of the quantum interference realized in plasmonic waveguides is below 50% [12], which is the boundary between classical and quantum interference. This low visibility is not compelling evidence that single plasmons are usable for quantum information processing. Interference visibility is so important that higher quantum interference visibility implies higher operation fidelity and a higher probability of success. For example, the HOM interference with 95% visibility

that can be achieved in QPICs based on dielectric waveguides is used to realize quantum controlled-NOT gates [1]. Second, loss is unavoidable in QPICs that are based on plasmonic waveguides [4], owing to the absorption of metals. Although the properties of lossy quantum channels have been recently observed and studied in the context of free-space quantum optics [13, 14], the influence of such losses on quantum processing using QPICs remains unknown [15, 16].

The current study experimentally achieved the on-chip quantum interference of single plasmons using dielectric-loaded plasmonic waveguides at telecom wavelengths. The visibility was as high as $95.7 \pm 8.9\%$, which unambiguously demonstrates the bosonic nature of single plasmons and paves the way for the performance of basic quantum operations in plasmon-based QPICs. Furthermore, an SPP waveguide might provide a perfect testing ground for studying lossy photonic devices owing to the relatively high loss of such a device compared with dielectric devices. Our analysis indicates that sub-wavelength plasmonic components can be used as quantum devices for QPICs only when the loss effect is carefully addressed because loss can significantly reduce quantum interference visibility. Because loss is inevitable in waveguides, it is necessary to consider its influence on quantum coherence when designing QPIC structures.

Results

The principle of quantum interference. HOM interference, a basic type of quantum interference that reflects the bosonic properties of a single particle, is generally used to test the quantum properties of single plasmons [10]. In addition to its fundamental importance within quantum physics, the HOM effect underlies the basic entanglement mechanism in linear optical quantum computing [17] because two-qubit quantum gates, which form the core of linear optical quantum computing, can be obtained via classical and quantum interference (HOM interference) effects followed by a measurement-induced state projection.

*renxf@ustc.edu.cn

†bhliu@ustc.edu.cn

‡gpguo@ustc.edu.cn

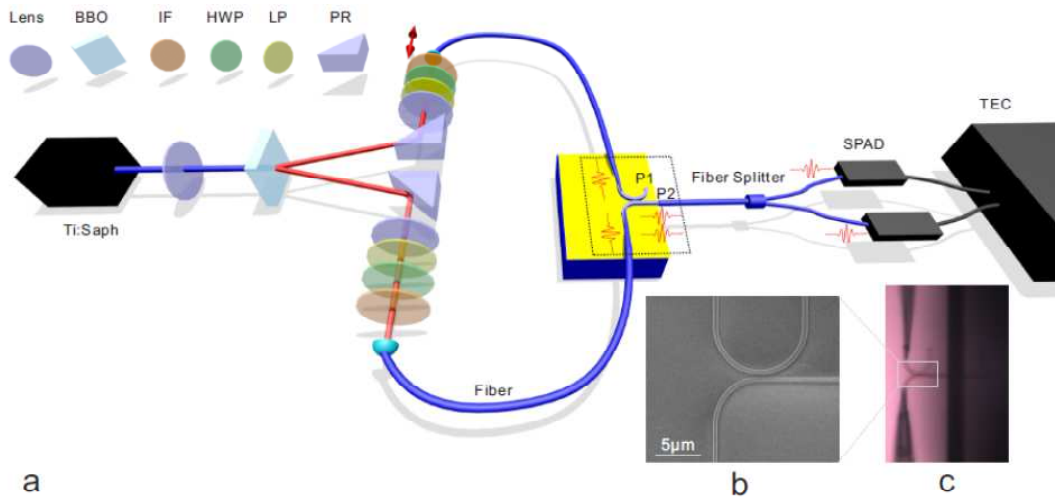


FIG. 1: (a) Schematic of the experimental setup. Photon pairs are generated via a degenerate type-II non-collinear spontaneous parametric down-conversion (SPDC) process. A 1.5-W pump laser (775 nm, Coherent Inc.) is focused on a 1-mm-long BBO crystal. The produced twin photons (1550 nm) are separated in free space by a 6° angle based on the phase-matching condition and directed to different optical single-mode fibers. A motorized delay line in one of the arms allows the optical-path-length difference between the two photons to be controlled with 100-nm resolution. Using the fiber taper connected to the single-mode fiber, the single photons are converted into single plasmons in the plasmonic waveguide, which then interfere with each other. We collected the photons from P2 of the on-chip directional coupler (DC) and sent them to a second 50/50 fiber BS. Coincidence measurements revealed the quantum properties of single plasmons. (b) A scanning electron microscope (SEM) image of part of a typical plasmonic DC structure. (c) A CCD image showing the coupling of the fiber taper and the SPP waveguide. A single-mode fiber was used to collect the photons from P2 using the end-fire coupling method.

HOM interference can be described as follows: when two indistinguishable photons enter a 50/50 beam splitter (BS) from different sides at the same time, according to the exchange symmetry of photons (bosons), a 50% chance exists of obtaining two photons in output port 1 (P1); furthermore, a 50% chance probability exists of obtaining two photons in output port 2 (P2). However, the two photons will never be in different output ports. The twin photon state $|1, 1\rangle$ is converted into a quantum superposition state $1/\sqrt{2}(|2, 0\rangle + |0, 2\rangle)$. This phenomenon is a signal of photon bunching and can only be explained using a quantum mechanism [18]. Experiments typically control the arrival times of two photons by adjusting the path-length difference between them and measure the photon coincidence of P1 and P2. When two indistinguishable photons completely overlap at the BS, they give rise to the maximum interference effect, and no coincidence exists. Visibility is defined as $V_1 = (C_{max} - C_{min})/C_{max}$, where C_{max} is the maximum coincidence and C_{min} is the minimum coincidence. For perfect quantum interference, $C_{min} = 0$ and $V_1 = 1$, whereas for a classical coherent laser, $V_1 = 50\%$. Consequently, to prove that destructive interference is due to two-photon quantum interference, the visibility must be greater than 50%. Here, we used a modified HOM interferometer (see Figure 1a). We collected the photons from P2 of the first BS, sent them to the second 50/50 BS, and then measured the coincidence. According to quantum interference theory, a 25% chance should exist for us to record a click when HOM interference occurs and a 12.5% chance otherwise. In this case, visibility was modified as follows: $V_2 = (C_{max} - C_{min})/C_{min}$. For perfect quantum interference, $C_{max} = 2C_{min}$ and $V_2 = 1$. Our modified interferometer is capable of reflecting the indis-

tinguishability of the input particles and can tell us whether these plasmons are bosons.

Experimental design. In the current experiment, we chose a dielectric-loaded SPP waveguide (DLSPPW) [19] to test the bosonic properties of the single plasmons. A DLSPPW is a typical sub-wavelength plasmonic waveguide that is formed by placing a dielectric ridge on top of a thin metal layer. Among the various plasmonic-waveguide structures, DLSPPWs are promising for enriching the functional portfolio of plasmonics owing to their dielectric-loading properties, which have been demonstrated in practice. They can confine the lateral size of propagating modes to the sub-wavelength scale and simultaneously transmit photons and electrons in the same component. In addition, because the energy is mostly confined to the surface of the metal, highly efficient control of the waveguide-mode characteristics is possible. For example, power-monitoring [20] and switching [21] elements with high response speeds have been experimentally demonstrated in DLSPPWs. We used nanofabrication techniques to prepare our plasmonic waveguide. Specifically, our waveguide was constructed of polymethyl methacrylate (PMMA) and placed on top of a 45-nm-thick gold layer deposited on a SiO_2 substrate. Figure 1b shows a scanning electron microscope (SEM) image of part of the fabricated sample.

Based on our calculations, the lateral size of the single-mode DLSPPW for photons at 1,550 nm was $600\text{nm} \times 600\text{nm}$ [22], because such a waveguide supports only one fundamental mode (see Figure 2b). The BS is realized using a directional coupler (DC), which is composed of two waveguides. In the coupling region, the evanescent fields of the two waveguide modes couple with each other and exchange energy. As

a result, two new coupling eigenmodes, the symmetric (Figure 2c) and anti-symmetric (Figure 2d) superpositions of the two waveguide modes, are generated. Owing to the different effective refractive indices of these two modes, the beating of the two modes leads to a BS-like function. By controlling the coupling strength, the amount of output at the two waveguide ports (the splitting ratio) can be tuned. Using the engineered waveguide gap, we obtained a coupling profile with a splitting ratio of approximately 1:1.

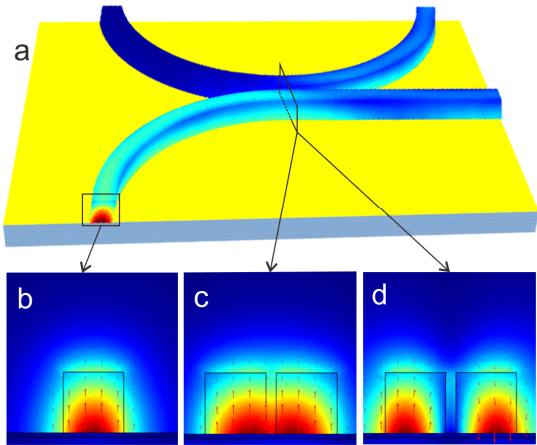


FIG. 2: (a) Three-dimensional simulation of field distribution on our plasmonic DC structure. (b) Field distribution in single mode plasmonic waveguide with lateral size of $600\text{nm}\times 600\text{nm}$. (c) Field distribution of symmetric eigenmode in coupling section. (d) Field distribution of anti-symmetric eigenmode in coupling section.

The coupling efficiencies among our SPP circuit, the external source, and the detectors were particularly crucial because the quantum signals were weak (approximately 7,000 photon pairs per second in our experiment). However, it is difficult to directly connect our plasmonic waveguide to a single-mode optical fiber because its lateral-mode field area is much smaller than that of the fiber (diameter $6.8\mu\text{m}$, 980HP, Thorlabs Inc.). Therefore, we adopted the alternative adiabatic method [5, 23] to excite the plasmons using fiber taper [24, 25]. As Figure 1c shows, the photons in the fiber are adiabatically squeezed into the microfiber via the taper region and coupled to the plasmon waveguide when the microfiber approached the waveguide. Owing to the high efficiency conversion and evanescent field coupling, the ideal conversion efficiency might have been higher than 99%. Under the limitations imposed by the experimental conditions, the efficiency of our fiber taper coupling system was estimated to be approximately 30%. Importantly, the alignment direction of the fiber taper was vertical to the collection fiber, thereby avoiding the collection of directly scattered photons from the end of the fiber taper.

Quantum-interference results. The 1,550-nm quantum photon pairs were generated via the spontaneous parametric down-conversion (SPDC) [26] process of a BBO crystal (Type-II phase matching, non-collinear) pumped by a 775-nm-wavelength laser (Coherent Inc.; see Figure 1a). The

down-converted twin photons consisted of one photon in the horizontal (H) polarization and one in the vertical (V) polarization. The photons were separated into two paths, each of which contained a prime reflector (PR), a half-wave plate (HWP, 1,550 nm), a long-pass filter (LP; 830 nm), and a narrow-band filter (IF, 1,550 nm, 8.8 nm FWHM). After these components, the two photons, which now had the same polarization, were guided into two separate single-mode fibers. One of the fiber couplers was installed on a motorized stage to adjust the optical path.

As shown in Figure 3a, the indistinguishability of the produced photon pairs was first characterized using a standard HOM interferometer with a fiber BS. The dip represented the quantum interference of two photons that arrived at the BS simultaneously, and the coherence of the photons determined its width. The quantum-interference results were fit using $N_{HOM} = C \cdot [1 - V \cdot e^{-(\Delta\omega \cdot \Delta\tau)^2}]$ [10], where N_{HOM} is the measured coincidence count, C is a fitting constant, V is the quantum-interference visibility, $\Delta\omega$ is the bandwidth of the photons, and $\Delta\tau$ is the optical time delay. For perfect quantum interference of indistinguishable photon pairs, the visibility should be unity. Here, we obtained a visibility of $V = 95.5 \pm 1.0\%$ and an optical coherence length of $c/\Delta\omega = 162.6 \pm 5.0\mu\text{m}$, where c is the speed of light. The deviation of the visibility from 100% was attributed to the polarization distortion of the photons during propagation in the fiber, photon source variability, or both. We also tested the modified quantum interferometer, in which photons from one output port were divided using a second fiber BS and detected with two single-photon detectors. Fitting the experimental results (Figure 3b) using the function $N_M = C \cdot [1 + V \cdot e^{-(\Delta\omega \cdot \Delta\tau)^2}]$, we obtained a visibility of $96.5 \pm 3.1\%$ and a coherence length of $173.9 \pm 5.7\mu\text{m}$. These values were consistent with standard HOM interference.

Finally, we observed the quantum interference of single plasmons using the modified quantum interferometer, in which two single photons from the fiber excited plasmon pairs in separate waveguides, and quantum interference occurred in the coupling section. We sought to collect the two plasmons from the two output ports and record their coincidence with a standard HOM interferometer; to do so, we required two additional fiber tapers to collect the signal. To avoid this requirement, we simplified the experimental design by collecting the photons scattered from P2 using an end-fire-coupled single-mode fiber. Using the second fiber BS, we divided the collected photons into two ports and measured the coincidence. Three samples were measured, and the visibilities were $95.7 \pm 8.9\%$, $93.6 \pm 6.7\%$, and $93.1 \pm 16.5\%$. These values are well above the classical limitation of 50%. The coherence lengths of the plasmons were also calculated using the experimental data, yielding $191.6 \pm 17.6\mu\text{m}$, $193.0 \pm 13.0\mu\text{m}$ and $146.4 \pm 9.4\mu\text{m}$, which were similar values to those of the photons. Our results demonstrate that although the electron is a fermion, a single plasmon (i.e., the quasi-particle of a collective electron-density wave) acts as a boson. The high visibility also suggests that plasmonic structures can be used in QPICs.

Discussion. In this section, we address the second question: what is the influence of loss on quantum interference visibility? The inevitable loss of SPPs attenuates the ampli-

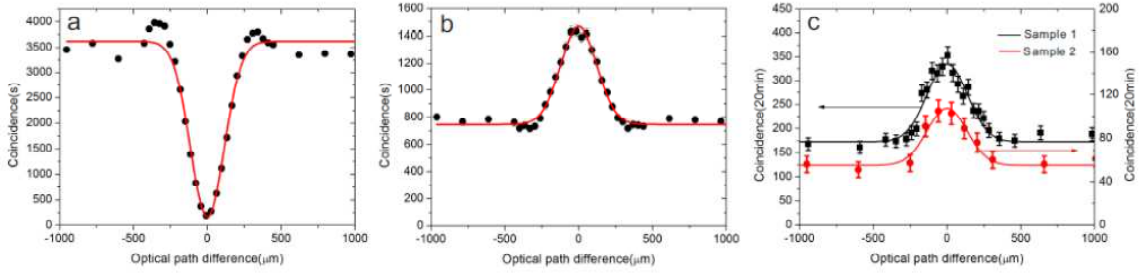


FIG. 3: (a) HOM interference of the down-converted photon pairs measured using a fiber 50/50 BS; the visibility was $95.5 \pm 1.0\%$ and the optical coherence length was $162.6 \pm 5.0\mu\text{m}$. (b) Modified HOM interference of the down-converted photon pairs measured using two fiber 50/50 BSs; the visibility was $96.5 \pm 3.1\%$, and the optical coherence length was $173.9 \pm 5.7\mu\text{m}$. (c) Quantum interference of single plasmons on DLSPPWs: For Sample 1, the visibility was $95.7 \pm 8.9\%$, and the optical coherence length was $191.6 \pm 17.6\mu\text{m}$; for Sample 2, the visibility was $93.6 \pm 6.7\%$, and the optical coherence length was $193.0 \pm 13.0\mu\text{m}$. All results are at the level of single photons.

tude of light; thus, gain materials are often used to compensate for this loss. In addition, the first-order coherence of the photons is destroyed during absorption and re-emission processes. It is necessary to determine how this loss influences second-order quantum interference visibility and under what conditions these losses are tolerable. The following discussion provides a detailed account of the two-photon quantum interference of lossy channels based on our plasmonic DC structure.

The operation of a four-port DC can be described as follows:

$$\begin{pmatrix} b_1^\dagger \\ b_2^\dagger \end{pmatrix} = \begin{pmatrix} r & t \\ t & r \end{pmatrix} \begin{pmatrix} a_1^\dagger \\ a_2^\dagger \end{pmatrix}, \quad (1)$$

where a_1^\dagger and a_2^\dagger as well as b_1^\dagger and b_2^\dagger are the creation operators of the input and output boson particles, and r and t are the amplitudes of the reflection and transmission coefficients. The output state of the input twin-particle state $|1, 1\rangle$ is

$$|\Phi\rangle_{out} = \sqrt{2}rt|2, 0\rangle + \sqrt{2}rt|0, 2\rangle + (r^2 + t^2)|1, 1\rangle \quad (2)$$

multiplied by a normalization factor. Here, we discard the terms that represent the loss of one or two particles because only the coincidence counts were recorded in the experiment. The probability of finding two particles in the same mode (proportional to the HOM interference visibility) is

$$P = \frac{4|rt|^2}{4|rt|^2 + |r^2 + t^2|^2}. \quad (3)$$

For a lossless system, the DC is characterized by its classical transmission and reflection coefficients, $|r|^2$ and $|t|^2$. Thus, designing a DC with $|r|^2 = |t|^2$ should optimize quantum interference. However, for a lossy system, the structures and microscopic transport process of the DC will determine the second-order quantum coherence. In our DLSPPW DC, when plasmons were propagated in the coupling region of the two waveguides, they were in coherent superpositions of symmetric and anti-symmetric modes (see Figures 2c and 2d). The precise microscopic losses can be included using the coeffi-

cients [27]

$$r = \frac{e^{in_2k_0L}}{2}(e^{i\text{Re}(\Delta n)k_0L}e^{-\text{Im}(\Delta n)k_0L} + 1) \quad (4)$$

$$t = \frac{e^{in_2k_0L}}{2}(e^{i\text{Re}(\Delta n)k_0L}e^{-\text{Im}(\Delta n)k_0L} - 1) \quad (5)$$

Here, $\Delta n = n_1 - n_2$, where $n_{1(2)}$ is the effective refractive index of the symmetric mode (the anti-symmetric mode), k_0 is the wave vector in free space, and L is the coupling length. The imaginary portion of $n_{1(2)}$ corresponds to the propagation loss of the plasmons and leads to a non-unitary operation matrix for the DC.

By substituting Eqs. (4) and (5) into Eq. (3), we obtain P , which is related to the loss difference between the two intermediate eigenmodes ($\propto \text{Im}(\Delta n)$) and the coupling length L . When L is sufficiently large, the energy in the eigenmode with higher loss approximates 0 and can therefore be neglected compared with the lower-loss eigenmode. In this case, P decreases to 0.5, which corresponds to a classical random process.

Figure 4 illustrates the relationships among P and L for a lossless DC (black dots), our DLSPPW DC (blue dots), and a metal-strip DC (red dots) in which we selected the L that corresponded to a 50/50 splitter. For a lossless DC, $P = 1$ for any selected L . In our sample, P slowly decreased as L increased. This result is because the difference between n_1 ($1.318 - 0.00426i$) and n_2 ($1.150 - 0.00437i$) is small; therefore, we were able to achieve a high interference visibility for a small L . For the metal-strip DC used in [12], P fastly decreased as L increased because the difference between n_1 ($2.036 - 0.02i$) and n_2 ($1.841 - 0.01i$) was much larger, especially in the imaginary portions.

The influence of loss on quantum coherence defined the limitations of lossy QPIC devices. The high-order quantum interference of photons should be considered when designing integrated photonic components because the microscopic processes of photons in these devices might deviate from the expected unitary evolution.

In summary, we experimentally demonstrated that single plasmons can be used as qubits to perform on-chip quantum information processing. The discussion presented here regarding loss also introduces a platform for using plasmonic

structures to investigate the on-chip quantum-decoherence phenomenon. Additional investigations should consider using single plasmons as qubits to carry quantum information and achieve on-chip linear optical computations or quantum simulations.

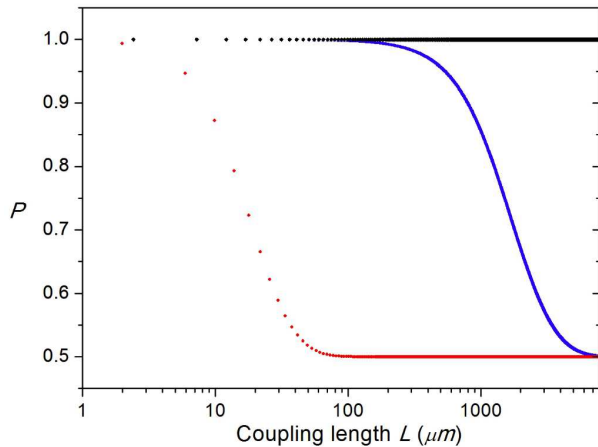


FIG. 4: The relationship between P and the coupling length L . The black, blue, and red dots represent the theoretical calculations for a lossless DC, our DLSPW DC and a metal-strip DC [12], respectively. R decreases as L increases and converges to 50% for sufficiently large L in lossy DCs. Here, we used the L values that corresponded to a 50/50 splitter.

Acknowledgments

This work was funded by NBRP (grant nos. 2011CBA00200 and 2011CB921200), the Innovation Funds from the Chinese Academy of Sciences (grant no. 60921091), NNSF (grant nos. 11374289, 10934006, 11374288, and 11104261), and NCET. We thank Prof. Fang-Wen Sun, Bao-Sen Shi and Zheng-Wei Zhou for useful discussion and Mrs Jun-Yi Xue from Qingdao No.2 High School of Shandong Province for her help in optical measurement.

-
- [1] Politi, A., Cryan, M. J., Rarity, J. G., Yu, S. & O'Brien, J. L. Silicaon-silicon waveguide quantum circuits, *Science* **320**, 646-649 (2008).
 - [2] Politi, A., Jonathan, C. F. M., O'Brien, J. L. Shor's Quantum Factoring Algorithm on a Photonic Chip. *Science* **325**, 1221 (2009).
 - [3] Barnes, W., Dereux, A. & Ebbesen, T. Surface plasmon sub-wavelength optics. *Nature* **424**, 824-830 (2003).
 - [4] Schuller, J. *et al.* Plasmonics for extreme light concentration and manipulation. *Nat. Mater.* **9**, 193-204 (2010).
 - [5] Zou, C. L. *et al.* Broadband integrated polarization beam splitter with surface plasmon. *Opt. Lett.* **36**, 3630 (2011).
 - [6] Dong, C. H., Zou, C. L., Ren, X. F., Guo, G. C. & Sun, F. W. In-line high efficient fiber polarizer based on surface plasmon, *Appl. Phys. Lett.* **100**, 041104 (2012).
 - [7] Altewischer, E., van Exter, M. P. & Woerdman, J. P. Plasmon-assisted transmission of entangled photons. *Nature* **418**, 304-306 (2002).
 - [8] Fasel, S. *et al.* Energy-time entanglement preservation in plasmon-assisted light transmission. *Phys. Rev. Lett.* **94**, 110501 (2005).
 - [9] Ren, X. F., Guo, G. P., Huang, Y. F., Li, C. F. & Guo, G. C. Plasmon-assisted transmission of high-dimensional orbital angular-momentum entangled state. *Europhys. Lett.* **76**, 753-759 (2006).
 - [10] Hong, C., Ou, Z. & Mandel, L. Measurement of subpicosecond time intervals between two photons by interference. *Phys. Rev. Lett.* **59**, 2044-2046 (1987).
 - [11] Fujii, G. *et al.* Preservation of photon indistinguishability after transmission through surface-plasmon polariton waveguide. *Opt. Lett.* **37**, 1535-1537 (2012).
 - [12] Reinier W. H., Leo P. K. & Valery Z. Quantum interference in plasmonic circuits. *Nat. Nanotechnol.* **8**, 719-722 (2013).
 - [13] Barreiro, J. T., Wei, T. C. & Kwiat, P. G. beating the channel capacity limit for linear photonic superdense coding. *Nat. Phys.* **4**, 282 (2008).
 - [14] Liu, B. H. *et al.* Experimental control of the transition from Markovian to non-Markovian dynamics of open quantum systems. *Nat. Phys.* **7**, 931 (2011).
 - [15] Stefano, L. Quantum simulation of decoherence in optical waveguide lattices. *Opt. Lett.* **38**, 4884-4887 (2013).
 - [16] Gupta, S. D. & Agarwal, G. S. Two-photon quantum interference in plasmonics: theory and applications. *Opt. Lett.* **39**, 390-393 (2014).
 - [17] Knill, E., Laflamme, R. & Milburn, G. J. A scheme for efficient quantum computation with linear optics. *Nature* **409**, 46 (2001).
 - [18] Lim, L. Y. *et al.* Generalized Hong-Ou-Mandel experiments with bosons and fermions. *New J. Phys.* **7**, 155 (2005).
 - [19] Kumar, A. *et al.* Dielectric-loaded plasmonic waveguide components: Going practical. *Laser Photonics Rev.* 1-14 (2013).
 - [20] Kumar, A. *et al.* Power monitoring in dielectric-loaded surface plasmon-polariton waveguides. *Opt. Exp.* **19**, 2972-2978 (2011).
 - [21] Kalavrouziotis, D., *et al.* Active plasmonics in true data traffic applications: Thermo-optic ON/OFF gating using a silicon-plasmonic asymmetric MZI. *IEEE Photon. Technol. Lett.* **24**, 1036-1038 (2012).
 - [22] Holmgaard, T., & Bozhevolnyi, S. I. Theoretical analysis of dielectric-loaded surface plasmon-polariton waveguides. *Phys. Rev. B* **75**, 245405 (2007).
 - [23] Zou, C. L. *et al.* Movable fiber-integrated hybrid plasmonic waveguide on metal film. *IEEE Photonic Tech. Lett.* **24**, 434-436 (2012).
 - [24] Dong, C. H. *et al.* Coupling of light from an optical fiber taper into silver nanowires. *Appl. Phys. Lett.* **95**, 221109 (2009).
 - [25] Guo, X. *et al.* Direct Coupling of Plasmonic and Photonic Nanowires for Hybrid Nanophotonic Components and Circuits. *Nano Lett.* **9**, 4515 (2009).
 - [26] Burnham, D. & Weinberg, D. Observation of simultaneity in parametric production of optical photon pairs. *Phys. Rev. Lett.* **25**, 84-87 (1970).
 - [27] Peter, N. T. *et al.* Integrated photonic sensing. *New J. Phys.* **13**,

055024 (2011).